Dalton Transactions

Accepted Manuscript

ROYAL SOCIETY OF CHEMISTRY

www.rsc.org/dalton

Cite this: DOI: 10.1039/c0xx00000x

www.rsc.org/xxxxxx

ARTICLE TYPE

BODIPY functionalized *o*-carborane dyads for low-energy photosensitization

Guo Fan Jin,[a] Yang-Jin Cho,[a] Kyung-Ryang Wee,[a] Seong Ahn Hong,[a] Il-Hwan Suh,[a] Ho-Jin Son,[a] Jong-Dae Lee,[*b] Won-Sik Han,[*c] Dae Won Cho,[*a] and Sang Ook Kang[*a]

Received (in XXX, XXX) Xth XXXXXXXXX 20XX, Accepted Xth XXXXXXXXX 20XX
DOI: 10.1039/b000000x

A new type of organic dyad that can induce low-energy photosensitization has been developed; electron donor and electron acceptor units are boron dipyrromethene (BODIPY) and ortho-carborane (*o*-Cb), respectively. New dyads consist of a V-shaped BODIPY-(*o*-Cb)-BODIPY molecular array in which two BODIPY units are substituted onto two adjacent carbon atoms of the central *o*-Cb. In the presence of *o*-Cb unit, as an electron acceptor, significant fluorescence quenching was observed which indicated photoinduced electron transfer (PET) had occurred from the end-on BODIPY units to the central *o*-Cb with PET efficiencies of 63~71%. As a result, corresponding cationic and anionic species that are responsible for the charge transfer state were detected by the serial spectroelectrochemical studies; cationic BODIPY radicals at 400 nm at the applied voltage of 1.44 V and broad absorption bands of anionic *o*-Cb radical in the range of 250 ~ 490 nm at –1.84 V. Transient absorption studies further confirmed the BODIPY radical anion at 540 nm and the *o*-Cb radical anion at 350–475 nm with structureless broad band.

Introduction

Electron donor-acceptor dyads have received much attention in the fields of solar energy conversion and storage,[1] molecular electronics,[2] photovoltaics,[3] and light-emitting diodes.[4] Especially, low-energy photo-sensitization is a key issue in the realization of solar light harvesting for highly efficient artificial photosynthesis systems[1] and solar cells.[3] To this end, porphyrin and its derivatives,[5] as well as other organic functional dyes including squarines,[6] were introduced. However, due to difficulties in their synthesis, alternate dyes have been investigated, and "boron dipyrromethene (BODIPY)" derivatives[7] are regarded as promising candidates based on the facts that they have been prepared by uncomplicated reaction procedures and, thus, were easily modified. Besides, they have high fluorescence quantum yield (60 ~ 90%), good chemical and photochemical stability, and adaptable charge-transfer properties. Most of all, they possess high extinction coefficients even at longer wavelength (40,000 ~ 110,000 M^{-1} cm^{-1} at ~500 nm) suitable to low-energy harvest.

Developing efficient electron acceptor (EA) units to harvest the maximum photons from solar radiation is of great importance in dyad systems. So far, functionalized fullerenes[8] and perylene bisimides[9] have been used as efficient EAs for the formation of the corresponding dyads. Recently, it has been reported that *ortho*-carborane (*o*-Cb) functioned effectively as an EA when two phenyl units are substituted at the cage-carbons.[10-12] We have reported that when engaging an electron donor (ED) to the Ph-*o*-Cb, a new type of *o*-carborane based dyad was formed in which ED was a carbazole (Cz) unit.[10] In this case, however, utility of the Cz-Ph-*o*-Cb dyad was limited since it was only photosensitized at high-energy (<350 nm).[13] Therefore, search for new electron donor within the realm of *o*-Cb EA enabling low-energy photosensitization is needed.

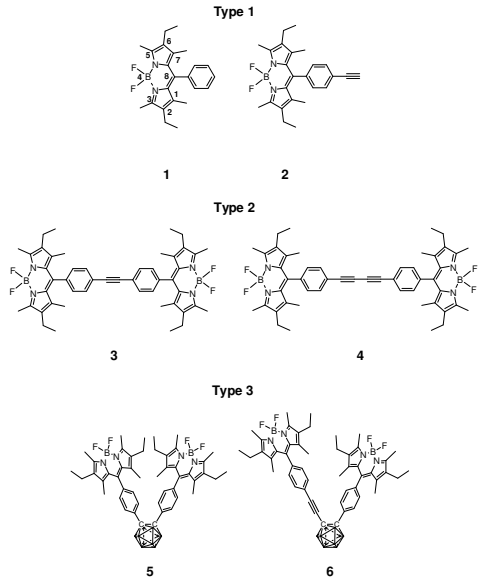

Chart 1 Molecular structure for BODIPY derivatives, **1**–**4**, and BODIPY-*o*-Cb dyads, **5** and **6**.

In this study, we report *o*-carboranyl dyads facilitated by the two BODIPY units for low-energy sensitization. To understand the

role of BODIPY-EDs to the *o*-Cb-EA, a stepwise comparative approach was undertaken by comparing parent BODIPY dyes with the structurally modified *o*-carboranyl BODIPY dyads. To investigate the role of *o*-Cb, compounds **5** and **6** in Chart 1 were prepared as BODIPY-*o*-Cb dyads and their photophysical properties were compared to those of the parent BODIPY dyes without *o*-Cb, **1**–**4** in Chart 1. Consequently, the following three different types of BODIPY derivative were studied: 1) phenyl-substituted BODIPY compounds with or without an acetylene unit (**1** and **2**), 2) *bis*-BODIPY compounds connected by either one or two acetylenic units (**3** and **4**), and 3) *o*-Cb based BODIPY dyads with or without internal acetylenic units (**5** and **6**). From comparative photophysical studies, fluorescence quenching was a dominant feature for the BODIPY-*o*-Cb dyads (**5** and **6**) and it was interpreted as photoinduced electron transfer (PET) process from BODIPY to *o*-Cb units. The PET process induced by attachments of *o*-Cb was investigated by fluorescence quenching, emission dynamics and time-dependent density function theory (TD-DFT) calculations to substantiate *o*-carboranyl dyad characteristics that withheld a charge transfer state below S_1 energy of the parent BODIPY. Furthermore, the photophysical properties of radical species generated via PET process were identified by the transient absorption (TA) measurements and confirmed by the spectroelectrochemical (SEC) analysis.

Results and discussion

The UV-Vis absorption and emission spectra of **1**–**6** in dichloromethane are shown in Fig. 1 and the corresponding data are summarized in Table 1. For **1** and **2**, the intense absorption band observed at ~530 nm is attributed to the $S_1 \leftarrow S_0$ (π–π^*) transition of the BODIPY unit (Fig. 1). The weak absorption band at approximately 400 nm can be assigned as a partially forbidden $S_2 \leftarrow S_0$ transition.[14] Since **3** and **4** have longer π-conjugation by the acetylene bridges, the absorbance at < 375 nm increases accordingly. The absorption intensities of **3**–**6** with two BODIPY units are approximately double those with one BODIPY unit in **1** and **2**. This indicates that **5** and **6** have negligible electronic coupling between BODIPY and *o*-Cb moieties in the ground state.

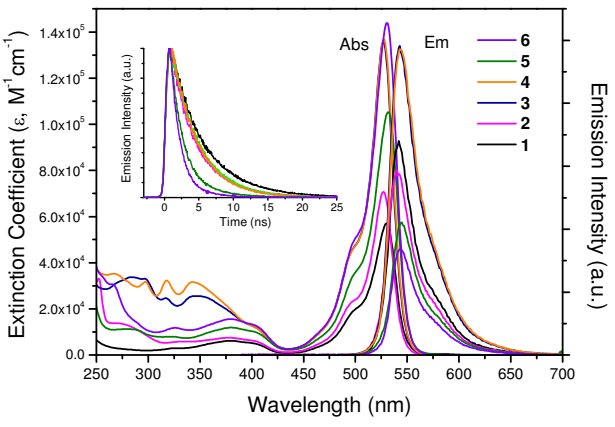

Fig. 1 Absorption and emission spectra of **1**–**6** (10 μM) in CH_2Cl_2 (λ_{ex} = 380 nm). Inset figure shows the fluorescence decay profiles for **1**–**6** in CH_2Cl_2 monitored at 550 nm at room temperature (λ_{ex} = 405 nm).

Table 1 Photophysical properties of Bodipy derivatives (**1**-**6**) in CH_2Cl_2

compounds	λ/nm, log ε/$M^{-1}cm^{-1}$	λ_f/nm[a]	τ_f/ns[b]	ϕ_f[c]
1	379 (3.8), 499 (4.3), 530 (4.8)	542	4.8	0.62
2	377 (3.9), 495 (4.4), 527 (4.9)	540	3.8	0.54
3	317 (4.4), 348 (4.4), 496 (4.7), 526 (5.2)	543	4.0	0.41
4	317 (4.5), 342 (4.5), 496 (4.7), 526 (5.1)	543	3.8	0.45
5	323 (3.9), 380 (4.1), 498 (4.5), 531 (5.0)	544	1.8	0.31
6	324 (4.1), 380 (4.2), 498 (4.7), 530 (5.2)	544	1.4	0.23

[a]λ_{ex} = 500 nm. [b]λ_{ex}= 408 nm. [c]reference: Rhodamine B (Φ= 0.49), λ_{ex} = 500 nm.

The emissions of **1**–**6** appear almost identical wavelength at around 540 nm but with different intensities. It is well known that BODIPY dyes have uniquely small Stokes shift, and exhibit high and environment-independent fluorescence quantum yields in many organic solvents. We also observed small Stokes shift with almost unchanged (<5 nm) absorption and emission bands maintained in various solvents of different polarity (Table S1 in ESI), because the dipole moment and transition dipole are orthogonal to each other.[15]

The molecular structure of **6** was determined by single crystal diffraction analysis and the molecular configuration is shown in Fig. 2. Selected crystallographic data and structure refinement parameters are summarized in Table S3 and S4 in ESI. In the crystal structure of **6**, as shown in Fig. 3, the dihedral angles between the BODIPY and the phenyl at the C(21) and C(45) positions of the BODIPY planes are in orthogonal positions with 91.3°(4) for C(19)-C(18)-C(21)-C(30) and 90.9°(4) for C(41)-C(42)-C(45)-C(46). Furthermore, two methyl groups at the C(26), C(34), C(50), and C(58) positions of the BODIPY unit make the BODIPY and phenyl planes orthogonal, leading to a weak electronic coupling between them. Such an interaction can be related to a lower absorbance for the S_2 state at < 430 nm. The torsional angle of C(1)-C(2)-C(39)-C(40) portraying the phenyl group conformation with respect to the C-C bond of *o*-Cb, is 125.8°(3) which deviates from 90°, because of the steric hindrance imposed by two BODIPY moieties facing each other through space (Table S4 in ESI).

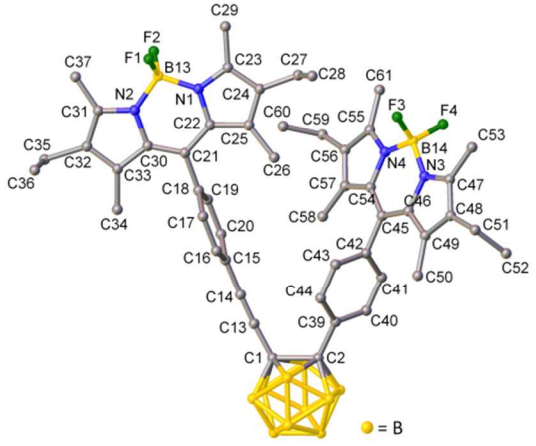

Fig. 2 Perspective views of crystal of **6** by using OLEX2.[16] Hydrogen atoms and solvent molecule CH_2Cl_2 were omitted for clarity.

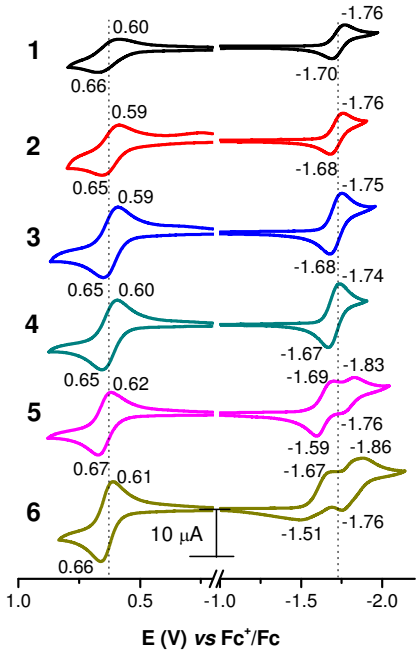

Fig. 3 Cyclic Voltammograms for 0.1 mM CH_2Cl_2 solution of **1**–**6** containing 0.1 M TBAP taken at a scan rate of 0.1 V/s.

To understand electrochemical properties, cyclic voltammetry (CV) was carried out using three-electrode cell system used comprised a platinum disk electrode as the working electrode, and a platinum wire and $Ag/AgNO_3$ as a counter and reference electrodes, respectively. As shown in Fig. 3, the CV spectra of **1**–**4** show reversible oxidation and reduction waves at the half-wave potentials of 0.62 ~ 0.63 V and –1.70 ~ –1.73 V, respectively (Table S2 in ESI). On the other hand, CV spectra of **5** and **6** show two reversible reduction waves and the first reduction occurring at *ca*. –1.64 V is assignable to the Ph-*o*-Cb unit[17] and the second reduction occurring at *ca*. –1.81 V is related reduction wave to BODIPY, as shown in Fig. S1.

Using the half-wave oxidation (E_{ox}) and reduction (E_{red}) potentials between the anodic and cathodic peaks, the driving force (ΔG_{PET}) for the PET process of **5** and **6** can be calculated using the following equation, $\Delta G_{PET} = E_{ox} - E_{red} - E_{00}$, where E_{00} is the excitation energy for S_1 and S_2 states, respectively. As shown in Fig. 1, **1**–**6** show two absorption bands in ground state. The absorption for a higher excited (S_2) state is observed at a shorter wavelength than 430 nm. The ΔG_{PET} values for the S_2 state are calculated to be –0.6 and –0.66 eV for **5** and **6**, respectively. The largely negative ΔG_{PET} values indicate that the PET process is energetically favourable from the S_2 state to give the charge transfer (CT) state. As discussed above, however, it is known that the S_2 state of BODIPY is usually deactivated very quickly through the internal conversion (IC) process to the lowest excited singlet (S_1) state.[14] Therefore, the PET from the S_2 state would take place competitively with internal conversion process. On the other hand, the ΔG_{PET} values for the S_1 state are determined to be –0.02 and –0.08 eV for **5** and **6**, respectively. These moderate negative ΔG_{PET} values imply that the PET process from the S_1 state is also favourable.

The PET process can be confirmed using the fluorescence quantum yields (ϕ_f) of BODIPYs and its dyads. The ϕ_f for **2**–**4** are relatively high in the range of 0.41–0.62 as listed in Table 1. Slightly lower ϕ_f of **2**–**4** to compare with **1** imply that either the acetylene units pull electrons away from the BODIPY units or the structures become non-rigid in the excited-state. On the other hand, when the *o*-Cb unit is incorporated into the system, significantly lower ϕ_f values are observed for **5** and **6** with 0.23 and 0.31, respectively; thus, the emissions of the BODIPY-*o*-Cb dyads are quenched by the PET process from the BODIPY to the *o*-Cb moiety.[18] Regardless of the excitation with 500 or 408 nm, which can be excited the BODIPY into either the S_1 or the S_2 state respectively, all fluorescence emissions were measured at same wavelength and their fluorescence quantum yields showed negligible excitation dependency.

On the other hand, the fluorescence lifetimes of BODIPY-*o*-Cb dyads are significantly shorter (τ_f = 1.8 ns for **5** and 1.4 ns for **6**) than those of the reference BODIPY (τ_f = 4.8 ns for **1** and 3.8 ns for **2**) and *bis*-BODIPY compounds (τ_f = 4.0 ns for **3** and 3.8 ns for **4**), as shown in inset of Fig. 1. Based on the lifetime constant of **1** as a reference molecule, the PET efficiencies of dyads in the S_1 state were determined by equation (1):

$$\varepsilon_{PET}(\%) = 1 - \left(\frac{\tau_f}{\tau_f^o}\right) \times 100 \quad (1)$$

where τ_f^o and τ_f refer to the fluorescence lifetimes of the reference (**1**) and dyads (**5** and **6**), respectively. Thus, the corresponding ε_{PET} values are calculated to be 63% (**5**), and 71% (**6**), respectively, which are calculated from the emission lifetimes monitored at 550 nm.

Based on ε_{PET} values, the rate constants of PET (k_{PET}) can be determined experimentally using the following equation (2):

$$k_{PET} = \frac{1}{\tau_f^o}\left(\frac{1}{(1/\varepsilon_{PET}) - 1}\right) \quad (2)$$

where τ_f^o is the fluorescence lifetime of donor (**1**) in the absence of the acceptor, the ε_{PET} is PET efficiency. Using equation (2), the k_{PET} values are estimated to 9.5×10^8 and 1.7×10^9 s^{-1} for **5** and **6**, respectively.

In order to understand the transition states, quantum chemical calculations (DFT/B3LYP/6-31G(d,p)) were carried out using *Gaussian 09* package.[19] The optimized geometry (*vide infra*) using DFT calculation shows excellent agreement with crystal structure of **6**. Therefore, even though we could not obtain the crystal structure of **5**, optimized geometry of **5** obtained from DFT calculation was used to compare the torsional angles of phenyl groups with respect to the C-C bond of *o*-Cb. Optimized geometries of **5** and **6** showed their torsional angles of 110.7° and 119.8°, respectively, between the phenyl group and the C-C bond of *o*-Cb. It is known that electron transfer can be facilitated from the phenyl to the *o*-Cb unit when directly substituted aryl groups are in orthogonal position to facilitate the π^*–σ^* orbitals overlapping in the excited state.[20] Thus, inclined torsional angle between C–C bond of *o*-Cb and directly substituted phenyl would interrupt electron transfer from the BODIPY to *o*-Cb unit in **6**. In compound **6**, however, acethylene bridged phenyl BODIPY unit which is another substituted group to the C–C bond of carborane cage can play a role for an efficient electron transfer from

BODIPY

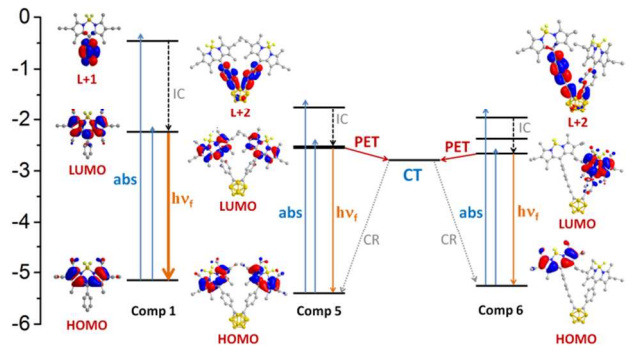

Fig. 4 Schematic energy diagram for the PET and recombination processes of BODIPY-*o*-Cb (IC: internal conversion, CR: charge recombination). Molecular-orbital patterns and energy levels of **1**, **5**, and **6** with the geometry of each molecule optimized at the B3LYP/6-31G(d,p) level of theory.

to *o*-Cb. Acetylene carbons have *sp* orbital with two filled pi orbital. Therefore, even though the torsional angle of C(2)-C(1)-C(13)-C(14) is 28.7°, σ^* orbital of C–C bond in *o*-Cb can be well-overlapped with one of π^* orbital in acetylene unit. The rationale for such interpretation is in good agreement with experimental results that the higher PET efficiency of **6** (ε_{PET} = 71%) than **5** (ε_{PET} = 63%).

The orbital diagrams for **1**–**6** also were estimated by DFT (B3LYP/6-31G(d,p)) calculations. In recent, it was reported that TD-DFT calculation contains serious low-accuracy for BODIPY moiety.[21] Also, we obtained poor absorption simulated by TD-DFT calculation as shown in Fig. S11, which showed large deviation compared to experimental absorption spectra. Moreover, for **5** and **6** dyads, the ordering of LUMO levels determined by DFT calculation seems lack of correlation with experimental results, because the orbital of LUMO (and L+1) should populate at o-Cb based on CV results. Therefore, we'd like discuss mainly for the explanation on orbital populations and transition states for **1**−**4**. The HOMOs of monomeric **1** and **2** are populated at the BODIPY moiety (Fig. S1 in ESI). Similarly, the LUMO is located at the BODIPY moiety, but the LUMO+1 (L+1) and L+2 for **1** and **2** are localized at the acetyl phenyl and/or phenyl groups, respectively. The absorption band for **1** and **2** at around 400 nm can be assigned as L+1←HOMO or LUMO←H–1 transition (Table S5 in ESI). The oscillation strengths for these transitions are relatively small, in accordance with the observed lower absorbance in the spectra of **1** and **2**. The lowest-energy absorption at around 530 nm is assigned as the LUMO←HOMO transition. In the cases of **3**–**6** (*bis*-BODIPY and BODIPY-*o*-Cb dyads), the HOMO and H–1 are degenerated, so are the LUMO and L+1, as shown in Fig. S1 in SI. Each orbital is distributed over the BODIPY moieties. Hence, the L+2 of **3**–**6** correspond to the L+1 of **1** and **2**. The L+2 for **3** and **4** are localized at the acetylene moiety, whereas those for **5** and **6** are extended to the *o*-Cb moiety.

Based on the fluorescence results, we propose that BODIPY-*o*-Cb dyad forms the charge transfer state *via* the PET process, which lies slightly below the S_1 state as revealed in Fig. 4. While the LUMO (or L+1) is localized in the BODIPY moiety, the upper L+2 for the dyad (**5**) and (**6**) are populated on the linkers and expanded to the *o*-Cb moiety.

In order to find out the spectral properties of radical species generated by the PET process, the SEC measurements were performed for **1**–**6** under constant voltage condition. After electrolysis at +1.44 V, which is the potential corresponding to the one-electron oxidation state (BODIPY$^{\bullet+}$), the SEC spectra of **1**–**6** shows absorption peak at the same position of around 400 nm as shown in Fig. 5a. It was reported that the absorption spectrum of an electrochemically oxidized BODIPY moiety exhibited a relatively weak absorption band around 380 and 515 nm which can be assigned to the radical cation of BODIPY, BODIPY$^{\bullet+}$.[22] Therefore, the observed at 400 nm band can be assigned to the BODIPY$^{\bullet+}$. However, the reported 515 nm band was not observed that might be due to strong bleaching of ground state absorption.

Since BODIPY moiety is only oxidized by this positive potential (+1.44 V), the transient SEC spectral features of **1**–**6** were almost identical at 400 nm. On the other hand, the radical anion species of BODIPY, BODIPY$^{\bullet-}$ was generated under negative potentials. Indeed, the SEC spectra for **1**–**4** taken after electrolysis at –2.14 V showed the transient bands at 320, 435 nm and 600 nm (Fig. 5b and Fig. S12 in SI). These peaks were enhanced upon electrolysis at a more negative potential, –2.29 V.

In case of **5** and **6** dyads, on the other hand, drastic changes in the SEC spectra were observed after electrolysis at negative voltages (Fig. 5c and Fig. S12 in SI). By varying the potential stepwise from –1.54 to –1.84 V, the SEC spectra for **5** and **6** showed very broad absorption bands in the range of 250 ~ 490 nm (Fig. 5c). This broad band is attributed to the reduced species of *ortho*-carborane (*o*-Cb$^{\bullet-}$).[13] This result indicates that the *o*-Cb moiety should be preferentially reduced at these potentials (–1.54 ~ –1.84 V). When **5** and **6** were electrolyzed at more negative potentials in the range of –1.94 ~ –2.29 V, the SEC spectra revealed noticeable increases of absorptions at 260, 350, 440 and 600 nm. These bands might be assigned as the absorption of BODIPY$^{\bullet-}$ and markedly enhanced according to increase of negative potential. In the condition of highly negative potentials, both moieties of BODIPY and *o*-Cb could be reduced, which may generate dianion species (**5**$^{2-}$ and **6**$^{2-}$, BODIPY$^{\bullet-}$-*o*-Cb$^{\bullet-}$) by sequential reduction. On the other hand, it seems that the BODIPY$^{\bullet-}$ has a larger extinction coefficient than *o*-Cb$^{\bullet-}$. Therefore, overall SEC spectral features of dianion species are similar to that of BODIPY$^{\bullet-}$ species.

Fig. 5d shows the transient absorption spectra for **1** and **5** in CH_2Cl_2 excited by the nanosecond laser-pulse at 355 nm. **1** shows the transient absorption band in the 400 ~ 500 nm, which is attributed to the T_1–T_n transition of the BODIPY chromophore.[23] Strong negative absorption occurred at around 530 nm is bleaching of the ground state absorption of BODIPY. The negative bleaching band was very strong compared with that of positive transient absorption band, because the extinction coefficient of BODIPY (^{3}BODIPY*) in the excited triplet may be extremely low. In case of **5**, the transient absorption spectrum shows structureless broad band at around 350–475 nm originated from the *o*-Cb$^{\bullet-}$ species. The peak of *o*-Cb$^{\bullet-}$ is generated simultaneously by photo-excitation through the PET process. Overall TA spectral features are quite similar to the SEC spectrum for **5** measured at –1.84 V. They are also similar to the

broad transient band centered at 380 nm for $Cb^{\bullet-}$ reported preivioulY.[13] Characteristic band for $Cb^{\bullet-}$ species is embossed on the TA spectra but not for $BODIPY^{\bullet+}$ species; this reflects very lower extinction coefficient of $BODIPY^{\bullet+}$ species as explained above. It is noteworthy that any discernable TA bands related to the $BODIPY^{\bullet-}$ species were found in photophysical process.

Conclusions

We have developed a new type of dyad incorporating low-energy sensitized BODIPY dyes into EA-*o*-Cb unit. As expected, BODIPY-*o*-Cb dyads were photosensitized by low-energy light and formed the corresponding CT state. The fluorescence intensities and lifetimes of BODIPY dyads were reduced much by presence of the EA-*o*-Cb unit through PET process. Fluorescence quantum yields measured by excitation in both S_1 and S_2 state confirm the PET process is mainly occurred from S_1 to CT states. The negative ΔG_{PET} value between S_1 and CT states clearly indicate that the PET from ED-BODIPY to EA-*o*-Cb is exergonic process. The transient species for $BODIPY^{\bullet+}$ and *o*-$Cb^{\bullet-}$ generated through the PET process are further investigated using the transient absorption measurement, and transient species, $BODIPY^{\bullet+}$ and *o*-$Cb^{\bullet-}$, are assigned based on the spectral data of SEC analysis. Finally, we conclude that the fluorescence quenching in BODIPY-*o*-Cb dyads system is originated from PET process and generated charge separated states are recombined with non-radiative decay process.

Experimental Section

General procedures

All manipulations were performed under a dry nitrogen atmosphere using standard Schlenk techniques or in a vacuum atmospheres glove box. Toluene was purchased from Samchun Pure Chemical Company and dried over calcium hydride before use. Glassware, syringes, magnetic stirring bars, and needles were dried in a convection oven overnight. Decaborane ($B_{10}H_{14}$) was purchased from Katchem and used after sublimation. The ^1H, ^{13}C, ^{11}B, and ^{19}F NMR spectra were recorded on a Burker 400 spectrometer operating at 400.1, 100.5, 128.4, and 376 MHz, respectively. ^1H and ^{13}C NMR chemical shifts were measured relative to internal residual peaks from the lock solvent (99.9% $CDCl_3$), and then referenced to $Si(CH_3)_4$ (0.00 ppm). All ^{11}B NMR chemical shifts were referenced to $BF_3{\cdot}O(C_2H_5)_2$ (0.0 ppm), with a negative sign indicating an up-field shift. Elemental analyses were performed using a Carlo Erba Instruments CHNS-O EA1108 analyser. IR spectra of samples were recorded on an Agilent Cary 600 Series FTIR spectrometer using KBr disks. Elemental analysis (Carlo Erba Instruments CHNS-O EA1108 analyser) and HR-MS (FAB) (Jeol LTD JMS-HX 110/110A) were performed by the Ochang branch of the Korean Basic Science Institute.

Synthesis details

Compounds **3** and **4** were synthesized according to the literature procedure.[24] Compounds **5** and **6** were prepared from decaborane and diethyl sulfide with compound **3** and **4**, respectively, at an elevated temperature of 80°C.[25] All products were isolated by flash column chromatography.

Compound 5: $B_{10}H_{12}(SEt)_2$ (0.17 g, 0.72 mmol) and **3** (0.57 g, 0.73 mmol) were dissolved in dry toluene (15 mL). The resulting mixture was stirred under N_2 for 2 h at 40˚C, then for 2 h at 60˚C, and then overnight at 80˚C. The organic layer was extracted with CH_2Cl_2 (3 × 30 mL) and dried over $MgSO_4$. The solvent was removed under reduced pressure and the residue was purified by silica gel column chromatography using CH_2Cl_2/hexane (1:1) as the eluent. **5** was obtained as a dark red powder (0.28 g, 43%). IR spectrum (KBr pellet, cm^{-1}): ν(B−H) 2581, 2601; ν(C–H, C=H) 2870, 2928, 2963. ^1H NMR ($CDCl_3$): δ 7.48-7.46 (d, J = 8.16 Hz, 4H), 7.08-7.06 (d, J = 8.0 Hz, 4H), 2.44 (s, 12 H), 2.15-2.09 (m, 8H), 1.02 (s, 12H), 0.81-0.76 (m, 12H) ppm. ^{11}B NMR ($CDCl_3$): δ 0.54, −2.68, −7.21, −8.82 ppm. ^{13}C NMR ($CDCl_3$): δ 154.7, 138.3, 137.8, 133.5, 131.9, 131.1, 130.4, 129.1, 129.0, 83.6, 17.2, 14.5, 12.7, 12.2 ppm. ^{19}F NMR ($CDCl_3$): δ −145.7 (d, J = 32 Hz, BF_2), −145.9 (d, J = 32 Hz, BF_2) ppm. HR-MS (FAB) calcd for $C_{48}H_{62}B_{12}F_4N_4$ (M^+) m/z 902.6027, observed 902.6014. Calcd for $C_{48}H_{62}B_{12}F_4N_4$: C, 64.00; H, 6.94; B, 14.40; F, 8.44; N, 6.22. Found: C, 64.02; H, 6.91; N, 6.18.

Compound 6: A procedure analogous to that used for the preparation of **5** was used. The starting materials were **4** (1.35 g, 1.67 mmol) and $B_{10}H_{12}(SEt)_2$ (0.48 g, 2.0 mmol). **6** was obtained as a deep red powder (0.78 g, 51%). IR spectrum (KBr pellet, cm^{-1}): ν(B−H) 2581, 2601; ν(C–H, C=H) 2850, 2920, 2959; ν(C≡C) 2234. ^1H NMR ($CDCl_3$): δ 7.85-7.83 (d, J = 8.0 Hz, 2H), 7.31-7.30 (d, J = 7.1 Hz, 3H), 7.18-7.16 (d, J = 8.7 Hz, 1H), 7.16-7.14 (d, J = 7.8 Hz, 2H), 2.44 (s, 12 H), 2.22-2.11 (m, 8H),1.12 (s, 6H), 1.11 (s, 6H), 0.92-0.82 (m, 12H) ppm. ^{11}B NMR ($CDCl_3$): δ 0.59, −3.34, −9.46 ppm. ^{13}C NMR ($CDCl_3$): δ 154.6, 138.7, 138.3, 138.1, 138.0, 137.8, 133.3, 133.0, 132.2, 131.7, 130.4, 129.0, 128.9, 120.4, 84.0, 82.9, 82.0, 77.4, 69.2, 17.3, 17.2, 14.8, 14.7, 12.7, 12.1, 12.0 ppm. ^{19}F NMR ($CDCl_3$): δ −145.6 (d, J = 36 Hz, BF_2), −145.8 (d, J = 32 Hz, BF_2). HR-MS (FAB) calcd for $C_{50}H_{62}B_{12}F_4N_4$ (M^+) m/z 926.6027, observed 926.6022. Calcd for $C_{50}H_{62}B_{12}F_4N_4$: C, 64.94; H, 6.76; B, 14.03; F, 8.22; N, 6.06. Found: C, 64.89; H, 6.74; N, 6.05.

Crystal structure determination

Crystals of **6** were obtained in a CH_2Cl_2/*n*-hexane solution, sealed in glass capillaries under argon, and mounted on a diffractometer. The preliminary examination and data collection were performed using a Bruker SMART CCD detector system single-crystal X-ray diffractometer equipped with a sealed-tube X-ray source (50 kV × 30 mA) using graphite monochromated Mo K_α radiation (λ = 0.71073 Å). The preliminary unit cell constants were determined using a set of 45 narrow-frame (0.3° in ω) scans. The double pass method of scanning was used to exclude noise. The collected frames were integrated using an orientation matrix determined from the narrow-frame scans. The SMART software package was used for data collection and SAINT was used for frame integration.[26] The final cell constants were determined through global refinement of the xyz centroids of the reflections harvested from the entire data set. Structure solution and refinement were carried out using the SHELXTL-PLUS software package.[27]

Steady-state absorption and emission measurements

The absorption and photoluminescence spectra were recorded on

an Agilent Technologies Cary 5000 and a Varian Cary Eclipse, respectively. The emission quantum yields of the BODIPY-*o*-Cb dyads were determined by comparative method for samples of five different concentrations (1～10 μM) using rhodamine B (ϕ_f = 0.49 in ethanol) as a reference standard.[28]

Fluorescence lifetime measurement

Emission-decay analysis was performed on a time-correlated single photon counting equipment (Picoquant, PicoHarp 300 using laser-diode 405 nm, 1 MHz, FWHM = ~100 ps). The instrumental response of the entire system was 50 ps, which resulted in a resolution of 10 ps after deconvolution.

Laser flash photolysis

The nanosecond transient absorption measurements were conducted using laser flash photolysis.[29] The samples were excited by third-harmonic generation (355 nm, FWHM of 4.5 ns) from a Q-switched Nd:YAG laser (Continuum, Surelite II-10). Light from a xenon arc lamp (ILC Technology, PS 300-1) was focused on the sample for the transient absorption measurements. Temporal profiles were measured with a monochromator (DongWoo Optron, Monora 500i) equipped with a fast photomultiplier tube (Zolix Instruments Co., CR 131) and a digital oscilloscope (Tektronix, TDS-784D). The reported signals were averaged 600 events to obtain satisfactory signal-to-noise ratios. The transient absorption spectra were measured with an intensified charge-coupled device (Ando, iStar).

Cyclic voltammetry (CV) experiment

The cyclic voltammetry experiments were performed using an electrochemical analyzer (Bioanalytical System Inc., BAS 100). The three-electrode cell system used comprised a platinum disk (dia. 1.6 mm) electrode as the working electrode, and a platinum wire and $Ag/AgNO_3$ as a counter and reference electrodes, respectively. Freshly distilled, degassed CH_2Cl_2 was used as the solvent with 0.1 M tetrabutylammonium perchlorate (TBAP) electrolyte as the supporting electrolyte. The potential values were calibrated with respect to the Fc/Fc^+ (Fc = Ferrocene) redox couple. To check the number of electrons transferred per molecule, a linear sweep voltammetry experiment using a carbon micro-disk electrode was performed.

Spectroelectrochemical (SEC) measurements

The absorption spectra of one-electron-reduced or one-electron oxidation species were taken by a SEC method using strands of 0.1 mm diameter Pt wire[30] as the working electrode, a Pt wire coiled around the porous glass tube as the counter electrode, and an $Ag/AgNO_3$ reference electrode in a porous glass tube (2 mm inside diameter, 3 mm outside diameter, 40 mm length). The solution containing sample (0.5 mM) and TBAP (0.1 mM) in a quartz cell was purged with Ar for 10 min. After electrolysis using the electrochemical analyzer (BAS 100), the absorption spectra were measured immediately using the absorption spectrophotometer equipped with photodiode array detector (Sinco, S-3100).

Theoretical Calculations

All the calculations were performed on the platform of the Gaussian 09 package.[19] The ground-state geometry has been fully optimized at the density function theory (DFT) level using the B3LYP functional and the 6-31G(d,p) basis set for all atoms. Isodensity plots (contour = 0.03 a.u.) of the frontier orbitals were visualized by Chem3D Ultra program. The excitation energies and oscillator strengths for the lowest 30 singlet–singlet transitions at the optimized geometry in the ground state were obtained in time-dependent (TD)-DFT calculations using the same basis set and functional as for the ground state.

Acknowledgements

This work was supported by a Korea University research grant 2011.

Notes and references

[a]*Department of Advanced Materials Chemistry, Korea University, Sejong 339-700, South Korea. E-mail: dwcho@korea.ac.kr, sangok@korea.ac.kr*
[b]*Department of Chemistry, Chosun University, Gwangju 501-759, South Korea. E-mail: jdlee@chosun.ac.kr*
[c]*Department of Chemistry, Seoul Women's University, Seoul 139-774, South Korea. E-mail: wshan@swu.ac.kr*

† Electronic Supplementary Information (ESI) available: CIFs for **6**. CCDC 977268. Selected TD-DFT calculation results. ^1H, ^{13}C, ^{11}B, and ^{19}F NMR spectra for **5** and **6**. See DOI: 10.1039/b000000x/

1 (a) A. Harriman, M. A. H. Alamiry, J. P. Hagon, D. Hablot, R. Ziessel, *Angew. Chem. Int. Ed.*, 2013, **52**, 6611–6615. (b) M. Urbani, K. Ohkubo, D. M. S. Islam, S. Fukuzumi, F. Langa, *Chem. Eur. J.*, 2012, **18**, 7473–7485. (c) J. E. Bullock, R. Carmieli, S. M. Mickley, J. Vura-Weis, M. R. Wasielewski, *J. Am. Chem. Soc.*, 2009, **131**, 11919–11929.
2 D. M. Guldi, *Angew. Chem. Int. Ed.*, 2010, **49**, 7844–7846.
3 (a) G. Bottari, G. d. l. Torre, D. M. Guldi, T. Torres, *Chem. Rev.*, 2010, **110**, 6768–6816. (b) A. Mishra, M. K. R. Fischer, *Angew. Chem. Int. Ed.*, 2009, **48**, 2474–2499.
4 (a) J. M. Hancock, A. P. Gifford, Y. Zhu, Y. Lou, S. A. Jenekhe, *Chem. Mater.,* 2006, **18**, 4924–4932. (b) G. Hughes, M. R. Bryce, *J. Mater. Chem.*, 2005, **15**, 94–107.
5 (a) M. J. Griffith, K. Sunahara, P. Wagner, K. Wagner, G. G. Wallace, D. L. Officer, A. Furube, R. Katoh, S. Mori, A. J. Mozer, *Chem. Commun.*, 2012, **48**, 4145–4162. (b) M. V. Martínez-Díaz, G. d. l. Torre, T. Torres, *Chem. Commun*., 2010, **46**, 7090–7108.
6 (a) L. Hu, Z. Yan, H. Xu, *RSC Advances*, 2013, **3**, 7667–7676. (b) S. Sreejith, P. Carol, P. Chithra, A. Ajayaghosh, *J. Mater. Chem.*, 2008, **18**, 264–274.
7 (a) H. –J. Xu, A. Bonnot, P. –L. Karsenti, A. Langlois, M. Abdelhameed, J. –M. Barbe, C. P. Gros, P. D. Harvey, *Dalton Trans*., 2014, **43**, 8219–8229. (b) B. Brizet, N. Desbois, A. Bonnot, A. Langlois, A. Dubois, J. –M. Barbe, C. P. Gros, C. Goze, F. Denat, P. D. Harvey, *Inorg. Chem.*, 2014, **53**, 3392–3403. (c) B. Brizet, A. Eggenspiller, C. P. Gros, J. –M. Barbe, C. Goze, F. Denat, P. D. Harvey, *J. Org. Chem*., 2012, **77**, 3646–3650. (d) T. Bura, P. Retailleau, R. Ziessel, *Angew. Chem., Int. Ed*., 2010, **49**, 6659–6663. (e) A. C. Benniston, G. Copley, *Phys. Chem. Chem. Phys*., 2009, **11**, 4124–4131. (f) G. Ulrich, R. Ziessel, A. Harriman, *Angew. Chem. Int. Ed.,* 2008, **47**, 1184–1201. (g) A. Loudet, K. Burgess, *Chem. Rev.,* 2007, **107**, 4891–4932.
8 (a) C. Z. Li, H. L. Yip, A. K. Y. Jen, *J. Mater. Chem.,* 2012, **22**, 4161–4177. (b) S. Fukuzumi, T. Kojima, *J. Mater. Chem*., 2008, **18**, 1427–1439.
9 (a) W. Jiang, L. Ye, X. Li, C. Xiao, F. Tan, W. Zhao, J. Hou, Z. Wang, *Chem. Commun*., 2014, **50**, 1024–1026. (b) J. Zhang, M. K. R. Fischer, P. Bäuerle, T. Goodson, III. *J. Phys. Chem. B*., 2013, **117**, 4204–4215.
10 K. R. Wee, Y. J. Cho, J. K. Song, S. O. Kang, *Angew. Chem. Int. Ed*., 2013, **52**, 9682–9685.
11 (a) A. González-Campo, A. Ferrer-Ugalde, C. Viñas, F. Teixidor, R. Sillanpää, J. Rodríguez-Romero, R. Santillan, N. Farfán, R. Núñez,

Chem. Eur. J., 2013, **19**, 6299–6312. (b) B. P. Dash, R. Satapathy, B. P. Bode, C. T. Reidl, J. W. Sawicki, A. J. Mason, J. A. Maguire, N. S. Hosmane, *Organometallics,* 2012, **31**, 2931–2935. (c) F. Lerouge, A. Ferrer-Ugalde, C. Viñas, F. Teixidor, R. Sillanpää, A. Abreu, E. Xochitiotzi, N. Farfán, R. Santillan, R. Núñez, *Dalton Trans*., 2011, **40**, 7541–7550. (d) B. P. Dash, R. Satapathy, E. R. Gaillard, K. M. Norton, J. A. Maguire, N. Chug, N. S. Hosmane, *Inorg. Chem.,* 2011, **50**, 5485–5493. (e) B. P. Dash, R. Satapathy, E. R. Gaillard, J. A. Maguire. N. S. Hosmane, N. S. *J. Am. Chem. Soc.,* 2010, **132**, 6578–6587.

12 (a) A. R. Davis, J. J. Peterson, *ACS Macro Lett*., 2012, **1**, 469–472. (b) J. J. Peterson, A. R. Davis, M. Were, E. B. Coughlin, K. R. Carter, *ACS Appl. Mater. Interfaces,* 2011, **3**, 1796–1799. (c) K. Kokado, A. Nagai, Y. Chujo, *Macromolecules,* 2010, **43**, 6463–6468. (d) J. J. Peterson, M. Werre, Y. C. Simon, E. B. Coughlin, K. R. Carter, *Macromolecules*, 2009, **42**, 8594–8598.

13 K. R. Wee, W. S. Han, D. W. Cho, S. Kwon, C. Pac, S. O. Kang, *Angew. Chem. Int. Ed.*, 2012, **51**, 2677–2680.

14 D. W. Cho, M. Fujitsuka, J. H. Ryu, M. H. Lee, H. K. Kim, T. Majima, C. Im, *Chem. Commun.*, 2012, **48**, 3424–3426.

15 J. Karolin, L. B. A. Johansson, L. Strandberg, T. Ny, *J. Am. Chem. Soc*. 1994, **116**, 7801–7806.

16 O. V. Dolomanov, L. J. Bourhis, R. J. Gildea, J. A. K. Howard, H. Puschmann, *J. Appl. Crystallogr*. 2009, **42**, 339–341.

17 K. Hosoi, S. Inagi, T. Kubo, T. Fuchigami, *Chem. Commun.*, 2011, **47**, 8632–8634.

18 (a) Y. Morisaki, M. Tominaga, Y. Chujo, *Macromol. Rapid Commun*., 2013, **34**, 1357–1362. (b) K. Kokado, Y. Chujo, *J. Org. Chem.,* 2011, **76**, 316–319. (c) K. Kokado, Y. Chujo, Y. *Dalton Trans.,* 2011, **40**, 1919–1923. (d) K. Kokado, A. Nagai, Y. Chujo, *Tetrahedron Lett.,* 2011, **52**, 293–296.

19 M. J. Frisch, G. W. Trucks, H. B. Schlegel, G. E. Scuseria, M. A. Robb, J. R. Cheeseman, G. Scalmani, V. Barone, B. Mennucci, G. A. Petersson, *et al*. Wallingford CT, 2009.

20 (a) L. Weber, J. Kahlert, L. Böhling, A. Brockhinke, H. G. Stammler, B. Neumann, R. A. Harder, P. J. Low, M. A. Fox, *Dalton Trans*., 2013, **42**, 2266–2281. (b) L. Weber, J. Kahlert, R. Brockhinke, L. Böhling, J. Halama, A. Brockhinke, H. G. Stammler, B. Neumann, C. Nervi, R. A. Harder, M. A. Fox, *Dalton Trans*., 2013, **42**, 10982–10996. (c) L. Weber, J. Kahlert, R. Brockhinke, L. Böhling, A. Brockhinke, H. G. Stammler, B. Neumann, R. A. Harder, M. A. Fox, *Chem. Eur. J*., 2012, **18**, 8347–8357. (d) L. A. Boyd, W. Clegg, R. C. B. Copley, M. G. Davidson, M. A. Fox, T. G. Hibbert, J. A. K. Howard, A. Mackinnon, R. J. Peace, K. Wade, *Dalton Trans*. 2004, 2786–2799.

21 H. Ünal, D. Gunceler, E. Mete, *J. Photoch. Photobio. A*. 2014, **278**, 14−18.

22 S. Hattori, K. Ohkubo, Y. Urano, H. Sunahara, T. Nagano, Y. Wada, N. V. Tkachenko, H. Lemmetyinen, S. Fukuzumi, *J. Phys. Chem. B* **2005,** *109,* 15368–15375.

23 S. Guo, L. Ma, J. Zhao, B. Kucukoz, A. Karatay, M. Hayvali, H. G. Yaglioglu, A. Elmali, *Chem. Sci*., **2014**, *5*, 489–500.

24 G. Ulrich, R. Ziessel, *J. Org. Chem.*, **2004**, *69*, 2070–2083.

25 D. M. Schubert, C. B. Knobler, P. A. Wegner, M. F. Hawthorne, *J. Am. Chem. Soc.*, 1988, **110**, 5219–5221.

26 SMART and SAINT; Bruker Analytical X-Ray Division: Madison, WI, 2002.

27 G. M. Sheldrick, SHELXTL-PLUS Software Package; Bruker Analytical X-Ray Division: Madison, WI, 2002.

28 K. G. Casey, E. L. Quitevis, *J. Phys. Chem.*, 1988, **92**, 6590–6594.

29 Y. J. Cho, K. R. Wee, H. J. Son, D. W. Cho, S. O. Kang, *Phys. Chem. Chem. Phys*. 2014, **16**, 4510–4521.

30 (a) W. R. Heineman, W. B. Jensen, *Electrochemistry, Past and Present* (ACS Symp. Ser. 390), 1989, chap. 30, p. 442. (b) O. Ishitani, M. W. George, T. Ibusuki, F. P. A. Johnson, K. Koike, K. Nozaki, C. Pac, J. J. Turner, J. R. Westwell, *Inorg. Chem.* 1994, **33**, 4712–4717.

Graphical Abstract

Bodipy-*o*-carborane dyads undergo photo-induced electron tansfer (PET) process under low energy visible light sensitization and their PET efficiencies are in 63 ~71 % range.